FASS: The full aperture seeing sensor

A.Guesalaga[*,1], J.Osborn[2], M.Sarazin[3], B.Neichel[4], S. Perera[2], R.Wilson[2]

[1]Pontificia Universidad Católica de Chile, 4860 Vicuña Mackenna, 7820436 Santiago, Chile
[2]Durham University, South Road, Durham, DH1 3LE, United Kingdom
[3]European Southern Observatory, Karl-Schwarzschild-Str. 2, 85748 Garching, München, Germany
[4]Laboratoire d'Astrophysique de Marseille, Aix Marseille Université, 13388 Marseille, France

ABSTRACT

We describe a novel technique atmospheric turbulence monitoring called FASS (full aperture seeing sensor) based on a low noise CCD detector. The method uses a Fourier processing approach that estimates the spatial frequency distribution of the scintillation images. This frequency approach samples the propagated images along pupil rings, making the frequency transformation circular, avoiding distortions due to the finite nature of the data. It is shown that aspects such as detector exposure time, opto-mechanical stability, detailed modelling of propagation, noise and star chromaticity, must be carefully addressed during the design and calibration stages.

Although only ground conjugation results are presented in this article, the technique is expected to operate in the generalized mode guaranteeing sufficiently large speckles (larger than the detector pixels). Pixel gains and offsets are effectively corrected, so they don't significantly influence the accuracy of the profile estimation.

Temporal correlations are also shown to provide complementary information not only on the layer wind velocity, but a coarse estimation of their altitude.

Factors limiting the accuracy of the method, such as chromaticity, turbulence strength, exposure time and vibrations are discussed. The method provides excellent performance in simulations and encouraging preliminary results from on-sky images acquired in campaigns at La Palma and Paranal sites. Comparison to coetaneous profiles estimated with the Durham Stereo-SCIDAR instrument (DSS) are analysed.

Keywords: Turbulence profilers, Low noise CCD detectors, Site testing

1. INTRODUCTION

Latest generation of low noise CCD detectors offers the possibility of developing atmospheric turbulence monitors based on the processing of high resolution images to replace the well-known MASS and DIMM techniques [1-4]. The approach we propose is shown below, where the light from the telescope's full aperture is transferred to the detector, generating three images; two for image motion measurements (images of the star) and one for scintillation estimation (images of the pupil). We call this method FASS (Full Aperture Scintillation Sensor) as in this setup the full aperture of the telescope is used.
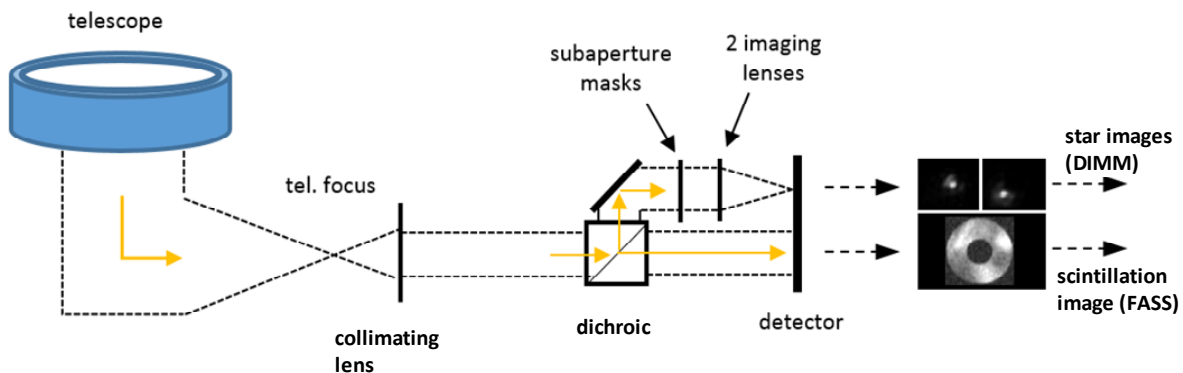

Figure 1. FASS configuration.

[*]aguesala@ing.puc.cl

The longitudinal and transversal image motion variances (S_l and S_t) calculated as described in the DIMM method [3], can be incorporated to the profile of FASS. Next, we focus on the altitude profiling to be estimated from the scintillation generated in the pupil image. It must be noted that DIMM channel is not strictly necessary, i.e. the extra complexity in the optics might not surpass its benefits when compared with a configuration of a single channel (scintillation), working in the generalized configuration (pupil conjugate below ground).

2. 2D FOURIER PROCESSING FOR THE PROFILE RECONSTRUCTION

An obvious approach to replace the standard concentric ring configuration of the original MASS method is to extract the speckle size and intensity information from 2D power spectra obtained from images of the full pupil, maximizing the use of the flux received by the telescope.

A mask has been applied to the simulated pupils in order to generate the same diffraction patterns as in the real case. The on-sky data has been recorded at the 1.0 m Jacobus Kapteyn Telescope (JKT) on La Palma.

A clear difference exists in the distribution of the power spectra, where smaller speckles populate higher frequencies whereas large speckles caused by high altitude turbulence will tend to concentrate the energy at the centre of the spectrum. This characteristic is used to generate the equivalent of the weighting functions in the new method by splitting the spectrum into concentric frequency rings that span the range of spatial frequencies generated by the speckles.
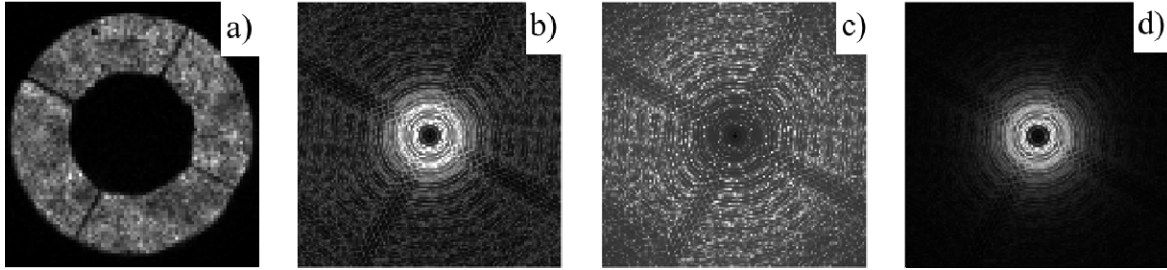

Figure 2. Images from pupil and 2D-power spectra of simulated and real (JKT). a) Pupil image of JKT with central obscuration and spiders; b) average 2D-PSD of JKT sequence c) simulation of a single layer at 500m; d) simulation of a single layer at 16,000m.

The next figure shows simulated pupil images of scintillation for the 1 m aperture of the JKT telescope caused by turbulence located at 500m and 10.000m respectively and for a seeing of 0.2". A clear distinction among the two cases are obvious, with a speckle size that is proportional to the altitude of the layers that according to the Fresnel law would be $d_s = \sqrt{h \cdot \lambda}$, with h being the altitude of the layer and λ the wavelength of the source (here considered monochromatic at 500nm). So, for the two layers considered: d_s @ 500 = 1.6 cm and d_s @ 10000 = 7.1 cm.

The pixel size of the camera is 1.4 cm, which a key parameter; essential to separate the noise (read-out or photon noise) from the speckle information. This parameter limits the minimum altitude that the speckles can be reliably detected and in this configuration, speckles generated by turbulence layers below 500 m are not possible to distinguished from the noise, i.e. the pixel size is comparable or even larger the expected speckle average diameter.
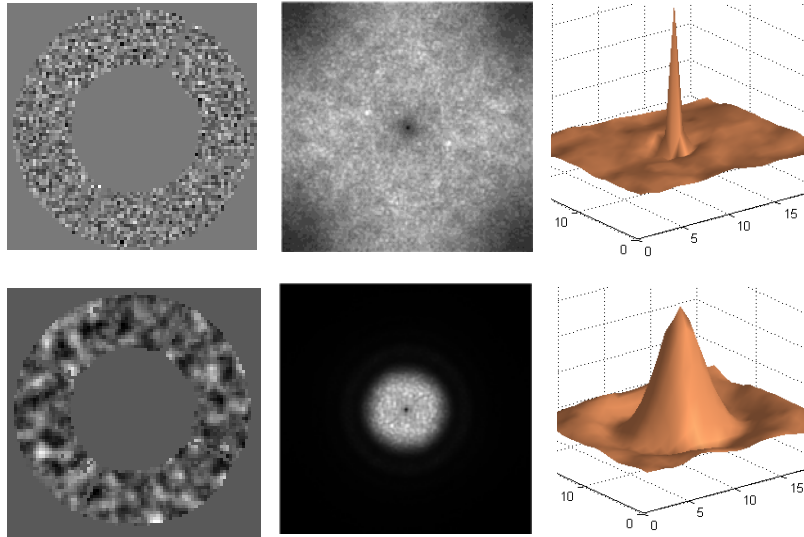
Figure 3. Speckles generated at the pupil; 2D power spectra of speckle images and autocorrelation functions of the pupil images by turbulent layers located at 0.5Km (left trio) and 10Km (right trio).

3. SOLUTION FOR SMALL TELESCOPES

One of the main objectives of this study is to evaluate this new approach in small telescopes. This is a key point as it would allow the development of low cost instruments.

Data from a telescope (Celestron C9.25 XLT, 23.5cm effective diameter) has been used in the following analysis. The pupil images below show two quite different cases of scintillation during the nights of September 27th and 29th, 2015. Notice that in the first case the image is populated with speckles of around a couple of pixels and in the second case, two different type of speckles appear: a low spatial frequency pattern (from higher altitude layers) and a high frequency one. The latter could be either a low altitude layer or just noise.
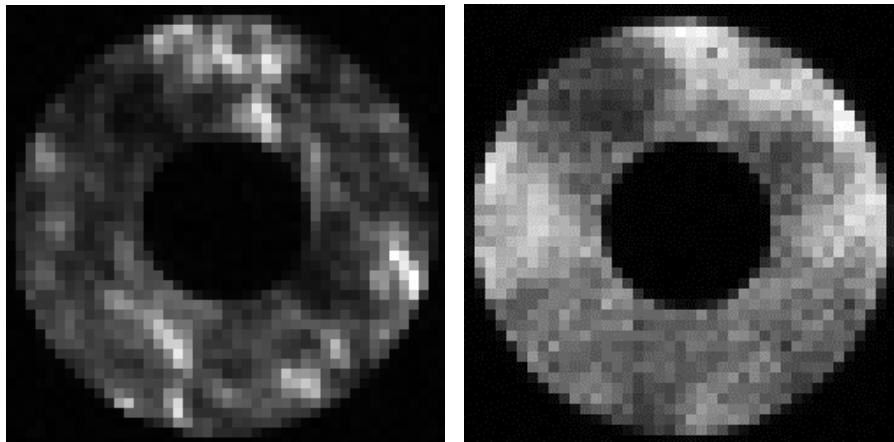

Figure 4. Two different cases of scintillation from on-sky data (September 27th and 29th, 2015); one dominated by low altitude turbulence (left) and the other with larger speckles corresponding to high altitude turbulence and a high frequency granulation due to noise or a low altitude layer

Figure 5 shows a simulated speckle image at the pupil generated by a turbulence layer at 18 Km (left) and an image from on-sky data (right). Notice that in both cases the speckles are comparable to the width of the pupil ring. A 2D processing would be impractical as these large speckles would generate an important amount of leakage in the frequency spectra due to the finite nature of the Fourier transform. However, by resampling the image along concentric rings in the pupil annulus (right), a longer length of the image data could be possible, were more than one of these large speckle could fit.

For example, a ring defined by a radius of $r = 10$ cm, would generate a sampled perimeter of $2\pi r \approx 60$cm, which can accommodate up to three complete cycles of 10 cm speckles (resulting after propagating a wavefront from a layer at 18Km).
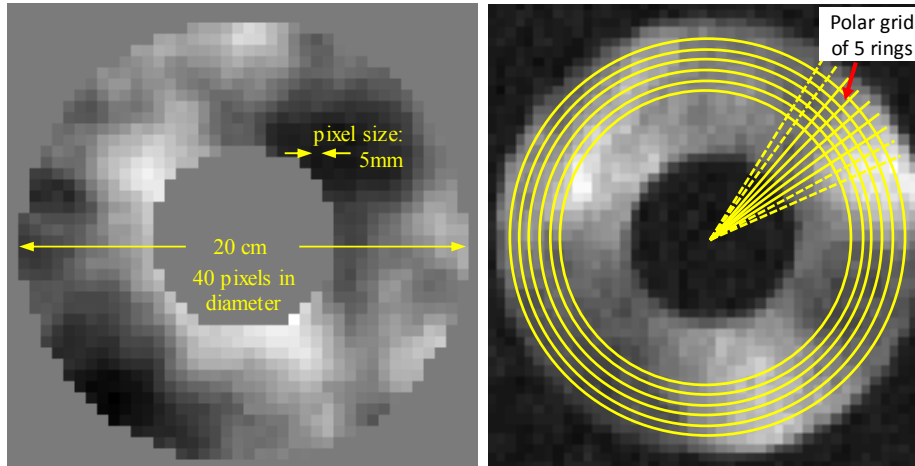

Figure 5. Pupil images for Celestron telescope. Left: simulation of a wavefront propagation from a layer at 18Km. Transformation from Cartesian to polar grid: example for three concentric rings with 128 divisions.

The benefits of unravelling the annulus is three-fold:

- It reduces the impact of diffraction rings from inner and outer pupil edges, especially at large negative conjugation altitudes

- Larger speckles can be detected (from higher altitude layer) due to sampling along the $2\pi r$ rings (r is the central radius of the resampled rings)

- The Fourier-transformed is performed for a circular, continuous 1-D vector

This resampling is described in Fig. 6. The Cartesian grid formed by the detector pixels is resampled via interpolation, using a polar grid that basically unravels one or more concentric rings. In the example, five rings that are unraveled to form a matrix of 128x5 pixels. The lines of this matrix (length 128) are Fourier transformed and later averaged.

It could be said that in the process of unbending the ring, the image is distorted. We found that this is not significant if the thickness of the rings is significantly lower than their diameter. The stretching of the outer rings would tend to cancel the effect of the compression of the inner ones.

Multiple single line rings covering the full aperture could be used. In this case however, the components of the resulting spectrum would have different values, so an average of the spectra is sought, a resampling of the spectra into a common frequency vector is necessary.

On the other extreme of the speckles side range, according to Fresnel law, the size of a speckle generated by a layer at 500m, would be around 1.7cm which is more than twice the size of the image pixel (pupil units), so pixel noise (readout or photon) should be possible to be differentiated from the smallest speckle for the layer at 500m.

By calculating the power spectra of each linear vector in the unravelled array and repeating this procedure for a large number of images, a spectrum is obtained for the profile estimation. In Fig. 7, 2,000 images of a propagated wavefront for layers at different altitudes have been processed. The 17 layer altitudes in this case are:

Z = [400 600 800 1200 1800 2400 3200 4200 5400 6800 8400 10200 12200 14400 16800 19400 23000]

The spectra generated by these 17 layers define the weighting functions, i.e. the equivalent to the MASS functions in [1]. We have found that not all the spectrum components are necessary for a good estimation, as all the spectral functions tend to converge to a common value at higher frequencies (except for the noise spectrum that remains constant).
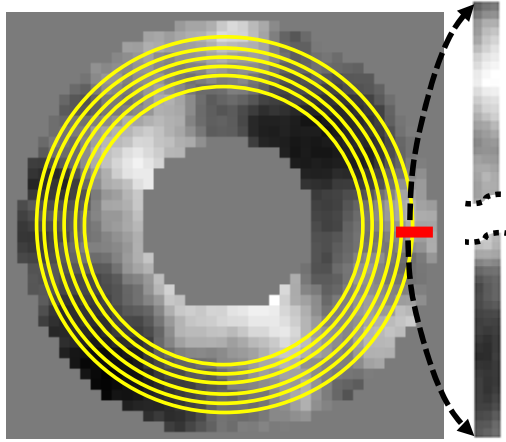
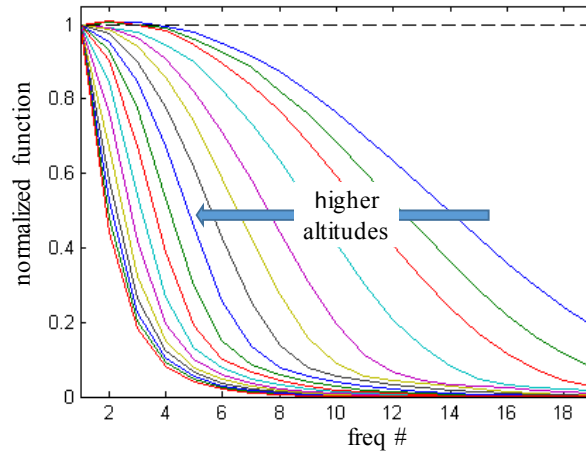Figure 6. Unraveling of a ring via interpolation from a 2-D Cartesian annulus to a linear array

Figure 7. Total of 17 valid weighting functions from the averaged spectra. Only the first 19 points suffice for a profile estimation

For the subsequent profile restoration, an inversion problem is stated as the minimization of the quadratic error between the measured spectrum and the combination of the previously computed spectra from individual layers (the weighting functions), located at the altitudes in Z.

Let's define:

$Z(i)$:   Location of the vertical slabs of the profile

$F_{cal}(i)$:   One dimensional average spectrum of rings for altitude $Z(i)$. This vector, contains frequency 19 elements (Fig. 7) and there are 17 vectors like this one; one per each altitude slab. The phasescreens used to compute them are simulated for three types of turbulence regimes: low (0.2" seeing); medium (0.5" seeing); and strong (0.8" seeing).

F_{meas}:   Same as before, but obtained from the detector data. A single 19-element vector is available in this case.

Mathematically, the profile is obtained by finding W such that $\quad J = \sum_{i=1}^{N_z} \left(a_f \cdot (F_{cal}^T \cdot W - F_{meas}) \right)^2 \quad$ is minimized.

Here $W=\{ w_i \}$ with $i = \{1, \ldots, N_z\}$, represents the profile. The value of N_z is 17 in our case. Coefficients in vector a_f (size 19) weigh the spectrum error in the minimization process in order to balance the integrated energy of each weighting function spectra. The differences in a_f are due to the large range of scintillation contrasts in the propagated

wavefronts propagated from higher altitudes compared to lower layers where a small scintillation occurs. We found that adequate values for these coefficients can be defined by taking the maximum values of the reference spectra for individual layers and later inverted. Figure 8 shows these 19 weighting values.
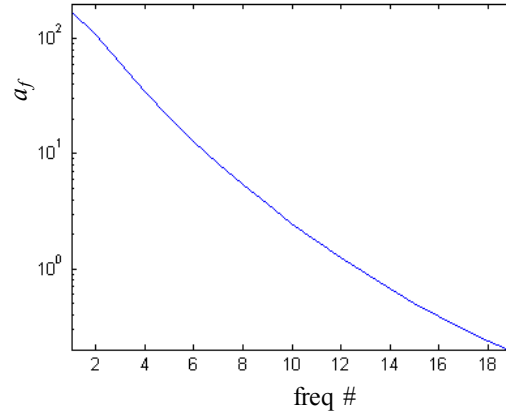

Figure 8. Weighting a_f for fitting minimization

Figure 9 shows the response functions for each of the 17 slabs computed from light propagated through individual layers at different altitudes. A clear improvement is observed when compared to MASS responses shown on the right panel.
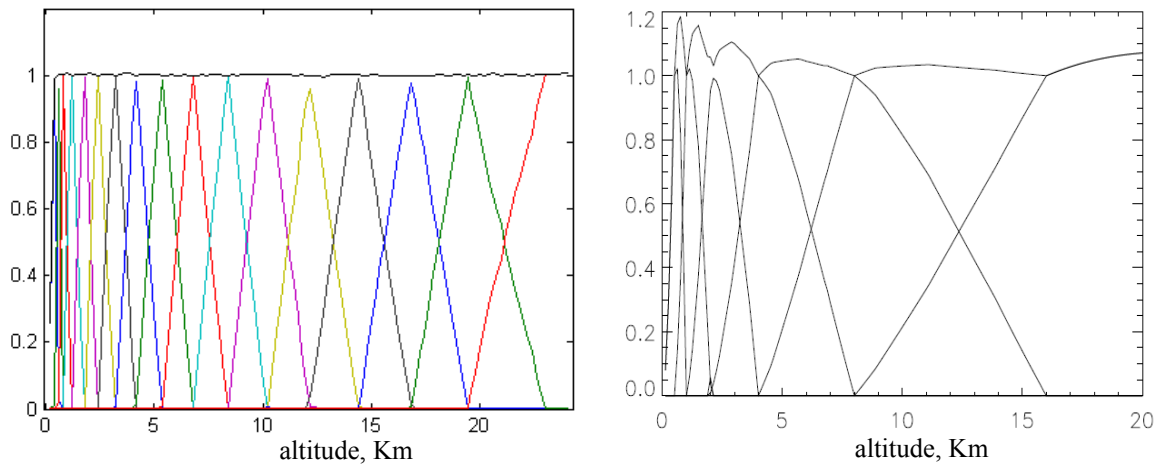

Figure 9. Left: FASS Response for 17 slabs. Right: Classical MASS response for 6 slabs (credit: Kornilov et al, 2003)

3.1 System set-up

Data have been collected from a campaign carried out at Paranal between the nights of April the 27th and 30th, 2016. The data from pupil images conjugated at the ground are accompanied by profiles obtained with a Durham Stereo Scidar (DSS) instrument [5] installed in one of the 1.8m auxiliary telescope (AT), about 20m away from the Celestron telescope. Profiles from DSS are approximately contemporaneous to each FASS profile.

The DSS instrument is conjugated at -3Km, so it provides good estimations of turbulence at the ground. Unfortunately, no complete comparison with our technique can be made as no reliable estimations at the ground exists for the FASS technique (conjugation at 0Km).

For the DSS profiler, binary stars were probed. For FASS, five different target stars were used: Altair, Canopus, Spica, Menkent and Miaplacidus. It must be bear in mind that the sky zone probed by each of the techniques are not the same, with large differences in both azimuth and zenith. This is essential to interpret the results obtained in each of the profiling methods.

During this campaign, the following set-up was used to collect the images:

Telescope: Celestron C9.25 XLT, 23.5cm diameter; focal length = 2350mm (f/10); collimator focal length = 15mm; beam size 1.5mm. The detector was placed conjugate to telescope pupil. No filter was used.

Camera: Andor Luca-S EM-CCD, with 10μm pixels, 4x4 binning (40μm effective pixel size) with and exposure time of 1 msec; frame rate of 200 Hz for full frames (658x496 pixels) and a binning of 4x4 pixels.
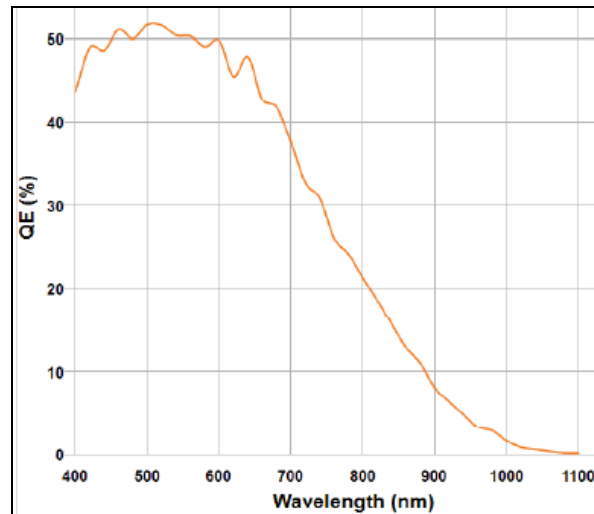

Figure 10. Andor Luca: quantum efficiency curve

Dichroic: Comar 590IK125, used at 45° angle with 50% transmission/reflectance at 550nm. Wavelengths above 550nm were sent to FASS and the lower part was used for total seeing (DIMM)
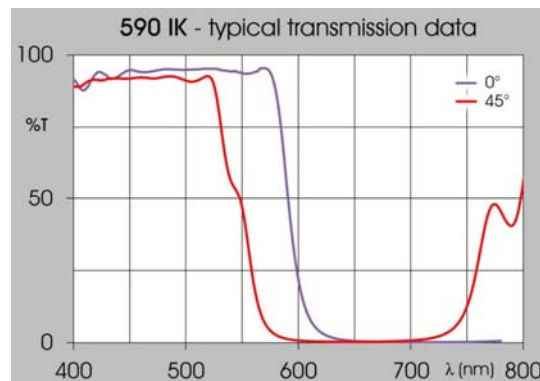

Figure 11. Dichroic spectral response (Comar, part 590IK125), used at 45° angle with 50%@550nm transmission

Weighting functions must be computed for each combination of star spectrum and detector and dichroic spectral transmissions given in Figures 10 and 11. Although this computation is a time-consuming process, it is not relevant as these reference functions can be pre-calculated and stored for later use.

3.2 Possible sources of error

We have found four possible causes of significant estimation errors. These are:

- Pixel size: an optical instability that causes an enlargement/shrinkage of the pupil image on the detector or aperture vignetting can cause a proportional variation of the speckle sizes (d) that according to Fresnel law ($h = d^2 / \lambda$) will produce a variation of the associated altitude layer of the square of such variation, e.g. a 10% error in the pixel size, will generate an overestimation of the layers altitudes 21%.

- Defocus: a deviation in the desired conjugate altitude will generate out-of-focus speckles with broader sizes, and hence an overestimation of altitudes.

- Detector integration time: Due to wind or telescope vibrations, the speckles will move during the integration time. For strong winds or high frequency vibrations, the speckles will smear out, broadening their sizes and causing an additional cause of altitude overestimation. For example, a wind of 10m/s will generate a displacement of the speckle during a 1ms integration time equivalent to 10mm. In our case this corresponds to more than half the size of a speckle generated by a layer at 500m. The effect can be significant for lower altitude layers. Integration times shorter than 1ms are very desirable, provided that the target star is sufficiently bright.

- Polychromatic light: A good modelling of the target star spectrum is a must. The simulated propagation must include all relevant wavelengths. Their combined effect generate speckle broadening that must be considered in the calculation of the reference functions.

4. RESULTS

Figure 12 present six examples of profiles observed during the three nights. In each plot, the yellow bars correspond to the profiles obtained with FASS together with the contemporaneous profiles obtained with the DSS approach. DSS profiles have been rearranged (integrated) over altitude segments that match the slabs of FASS. The zenith for each technique is written in the top-right corner of each panel.

Some results are good, but some are not. I must bear in mind that the values for zenith and azimuth are quite different for each instrument, so the differences are not surprising.

This is a small portion of the total number of images collected. A comprehensive analysis covering the full set of data is undergoing.
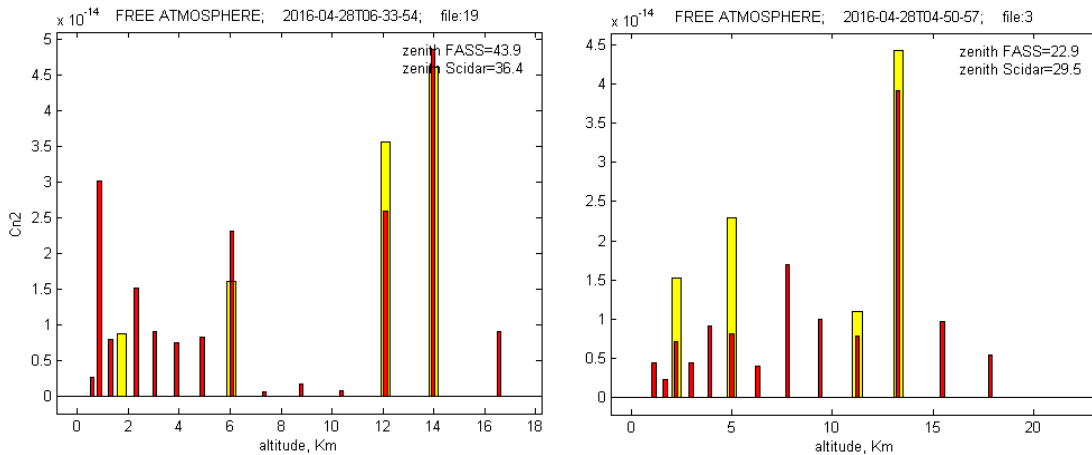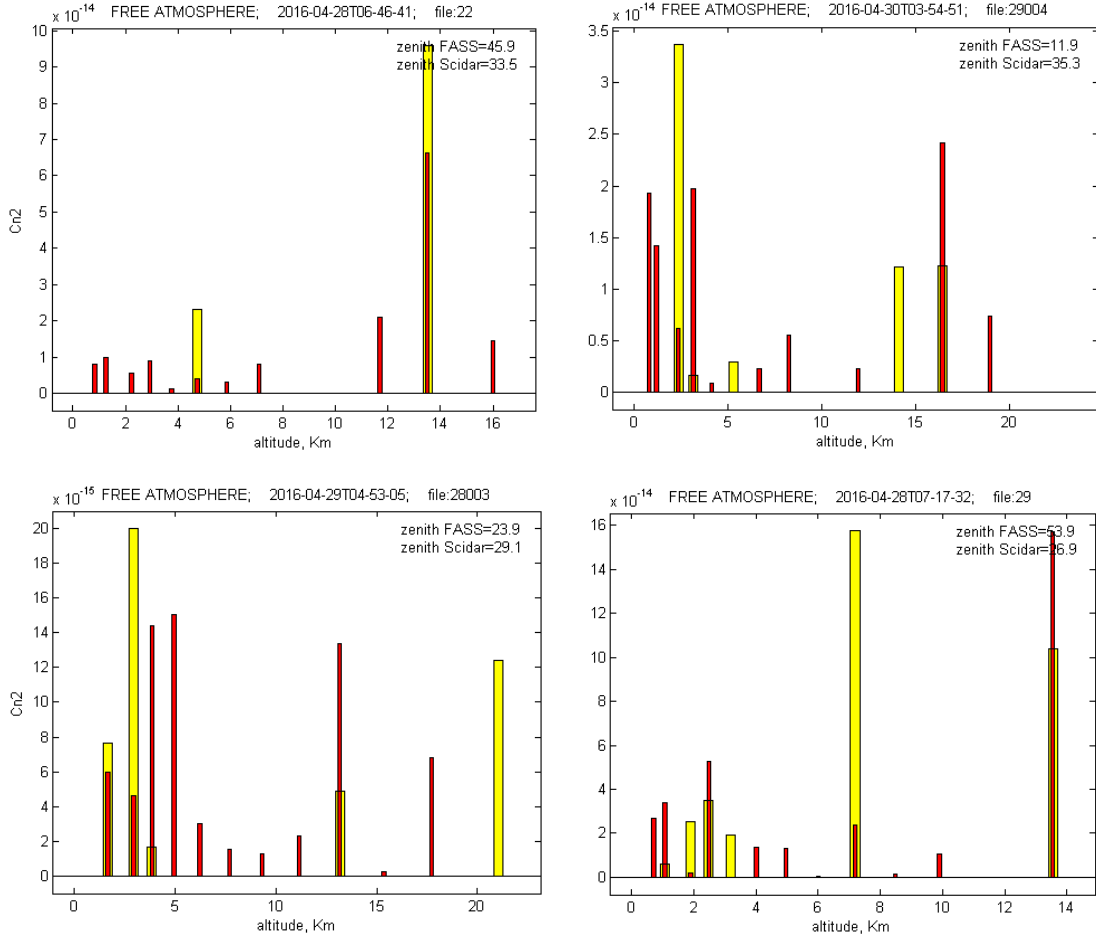
Figure 12. Six examples of profiles from the 3 nights (27/09/2014). The red thin bars are estimated by the DSS instrument and the yellow ones correspond to FASS

4.1 Temporal correlations

Figure 13 shows an example of the temporal analysis that can provide additional information on the speed of layers and their altitude. The top panel shows the FASS profile estimated for this case where at least two strong layers exist; one very close to the ground and the other around 4Km. This is also detected by the temporal correlations of the pupil images where two peaks, representing each layer are visible, moving at a speed of around 14m/s with slightly different directions. The width of these peaks provide information about their altitude. The small peak corresponds to the layer closer to the ground.
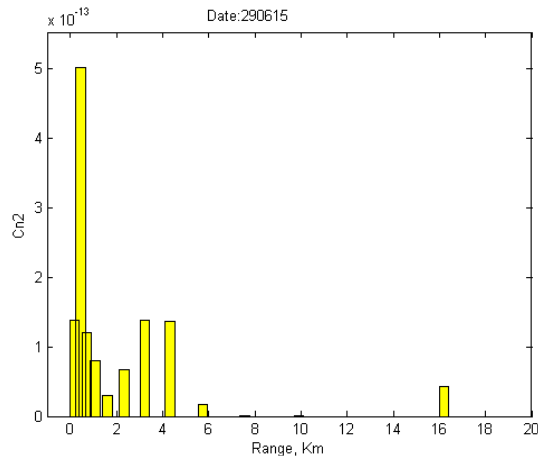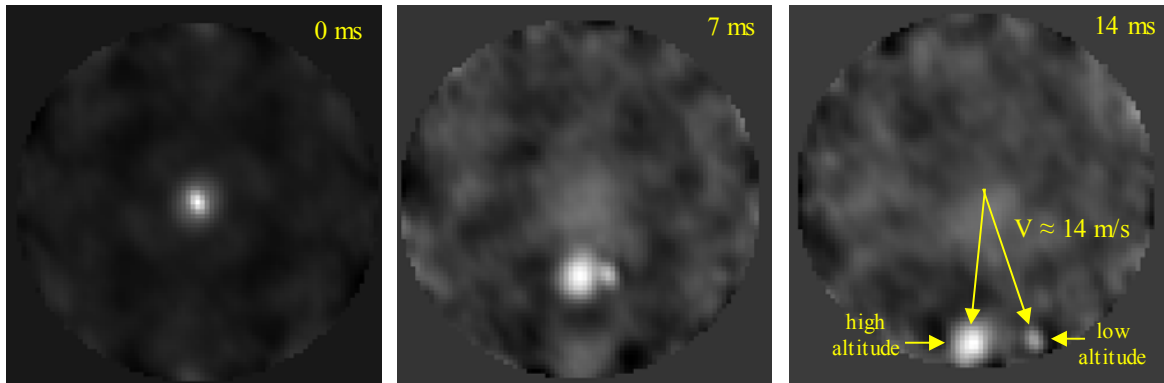
Figure 13. Temporal correlation sequence with two layers moving at similar speeds but different altitudes. Top: turbulence profile; Bottom: sequence of 3 steps for a frame rate of 140 Hz. Velocities near 14 m/s are calculated for both correlation peaks but moving with slightly different directions. The width of the peaks provides information about their altitude, i.e. the small peak corresponds to the layer closer to the ground.

Although this information is prone to severe errors due to change in wind velocity and disturbances such as vibrations, it can still provide qualitative information to confirm the existence of layers at the estimated altitudes in the profile by measuring the width of the autocorrelation function, which depends on the layer altitude (see Fig. 3).

5. CONCLUSIONS

The performance of the method based on the use of the full aperture of the telescope, with a single detector and a Fourier approach, show excellent results in simulations. Results from on-sky data and their comparison to profiles independently obtained with the DSS instrument look encouraging but not conclusive. To confirm the latter, further tests are required; in particular, pointing at the same sky area is necessary to probe the same turbulence. Configuring the optics to operate in the generalized mode is also necessary in order to have reliable estimations of the lower layers.

A revision of the optics specifications is needed. In particular, aspects such as detector integration time, opto-mechanical stability, detailed spectrum modelling of stars and detector response are required for good estimations. The use commercially available cameras with shorter integration time cameras with lower noise figures and higher quantum efficiency ratios should be investigated.

6. REFERENCES

[1] Kornilov V.,Tokovinin A.,Voziakova O.,Zaitsev A.,Shatsky, N.,Potanin S., Sarazin M., 2003, Proc. SPIE, 4839,837
[2] Tokovinin A., 2003, J. Opt. Soc. Am. A., 20, 686
[3] Tokovinin A., Kornilov V., 2007, MNRAS, 381, 1179
[4] Kornilov V., Tokovinin A., Shatsky, N.,Voziakova O., Potanin S., Safonov B., MNRAS, **382,** 2007
[5] Shepherd H.W., Osborn J., Wilson R.W., Butterley T., Avila R., Dhillon V.S. and Morris T.J., MNRAS, 2014

ACKNOWLEDGEMENTS